Published in final edited form as:
Sci Transl Med. 2010 April 7; 2(26): 26ra26. doi:10.1126/scitranslmed.3000502.

Klf15 Deficiency Is a Molecular Link Between Heart Failure and Aortic Aneurysm Formation

Saptarsi M. Haldar[1,*], **Yuan Lu**[1,*], **Darwin Jeyaraj**[1], **Daiji Kawanami**[1], **Yingjie Cui**[1], **Sam J. Eapen**[1], **Caili Hao**[1], **Yan Li**[2], **Yong-Qiu Doughman**[3], **Michiko Watanabe**[3], **Koichi Shimizu**[4], **Helena Kuivaniemi**[5], **Junichi Sadoshima**[6], **Kenneth B. Margulies**[2], **Thomas P. Cappola**[2], and **Mukesh K. Jain**[1,†]

[1]Case Cardiovascular Research Institute, Department of Medicine, Harrington-McLaughlin Heart and Vascular Institute, Case Western Reserve University School of Medicine, University Hospitals Case Medical Center, Cleveland, OH 44106, USA.

[2]Penn Cardiovascular Institute, 2 East Perelman Center for Advanced Medicine, 3400 Civic Center Boulevard, Philadelphia, PA 19104, USA.

[3]Department of Pediatrics, Rainbow Babies and Children's Hospital, Cleveland, OH 44106, USA.

[4]Donald W. Reynolds Cardiovascular Clinical Research Center, Cardiovascular Division, Department of Medicine, Brigham and Women's Hospital, Harvard Medical School, Boston, MA 02115, USA.

[5]Sigfried and Janet Weis Center for Research, Geisinger Health System, 100 North Academy Avenue, Danville, PA 17822, USA.

[6]Cardiovascular Research Institute, Department of Cell Biology and Molecular Medicine, University of Medicine and Dentistry of New Jersey, New Jersey Medical School, Newark, NJ 07103, USA.

Abstract

Current therapies for diseases of heart muscle (cardiomyopathy) and aorta (aortopathy) include inhibitors of the renin-angiotensin system, β-adrenergic antagonists, and the statin class of cholesterol-lowering agents. These therapies have limited efficacy, as adverse cardiovascular events continue to occur with some frequency in patients taking these drugs. Although cardiomyopathy and aortopathy can coexist in a number of conditions (for example, Marfan's syndrome, acromegaly, pregnancy, and aging), pathogenetic molecular links between the two

†To whom correspondence should be addressed. mukesh.jain2@case.edu.
*These authors contributed equally to this work.

SUPPLEMENTARY MATERIAL

www.sciencetranslationalmedicine.org/cgi/content/full/2/26/26ra26/DC1
Fig. S1. Cardiovascular abnormalities in AngII-treated mice and cultured cells.
Fig. S2. Baseline abnormalities in *Klf15*$^{-/-}$ heart and aorta.
Fig. S3. Cardiac mass and systolic blood pressure after AngII infusion.
Fig. S4. Histologic parameters in aortas.
Fig. S5. MMP-3 abundance in aortic smooth muscle.
Fig. S6. *p53* mRNA concentrations in heart and aortic tissue.
Fig. S7. p300 abundance in hearts, curcumin administration protocol, and aortic morphometry after curcumin therapy.
Table S1. Baseline cardiac parameters in *Klf15*$^{-/-}$ and wild-type mice.
Table S2. Cardiac parameters in *Klf15*$^{-/-}$ and wild-type mice after AngII infusion.
Table S3. Cardiac parameters in *Klf15* or *p53* compound mutant mice after AngII infusion.
Table S4. Cardiac parameters in curcumin-treated *Klf15*$^{-/-}$ and wild-type mice after AngII infusion.

diseases remain poorly understood. We reasoned that identification of common molecular perturbations in these two tissues could point to therapies for both conditions. Here, we show that deficiency of the transcriptional regulator Kruppel-like factor 15 (*Klf15*) in mice leads to both heart failure and aortic aneurysm formation through a shared molecular mechanism. *Klf15* concentrations are markedly reduced in failing human hearts and in human aortic aneurysm tissues. Mice deficient in *Klf15* develop heart failure and aortic aneurysms in a p53-dependent and p300 acetyltransferase–dependent fashion. KLF15 activation inhibits p300-mediated acetylation of p53. Conversely, *Klf15* deficiency leads to hyperacetylation of p53 in the heart and aorta, a finding that is recapitulated in human tissues. Finally, *Klf15*-deficient mice are rescued by *p53* deletion or p300 inhibition. These findings highlight a molecular perturbation common to the pathobiology of heart failure and aortic aneurysm formation and suggest that manipulation of KLF15 function may be a productive approach to treat these morbid diseases.

INTRODUCTION

Cardiac and vascular smooth myocytes respond to stress through tightly orchestrated gene-regulatory pathways (1,2). Dysregulation of these signaling pathways can drive pathologic tissue remodeling in the heart (cardiomyopathy) (1,3,4) and aorta (aortopathy) (5–8) and ultimately lead to organ failure. Progressive heart failure results in reduced blood flow to vital organs, fluid retention, and lethal cardiac rhythm disturbances. Deterioration of aortic integrity can lead to deadly complications, including aortic aneurysm formation (dilation of the aorta), rupture, and dissection (tearing of the aortic wall). Although cardiomyopathy and aortopathy can coexist in a number of conditions, including Marfan's syndrome, acromegaly, pregnancy, and aging (7,9–11), the pathogenetic molecular links between the two diseases are not known. We sought to identify common molecular perturbations occurring in these diseases of the two tissues. Given the residual morbidity and mortality associated with current treatment strategies for heart and vascular disease (7,12,13), the elucidation of such potential drug targets would be of clinical value.

Here, we show that deficiency of the transcriptional regulator Kruppel-like factor 15 (*Klf15*) occurs in human cardiomyopathy (3,4) and aortic aneurysms (14) and that deficiency of *Klf15* in mice (15) causes both cardiomyopathy and aortopathy in a p53-dependent and p300 acetyltransferase–dependent fashion.

RESULTS

Klf15 concentrations are reduced in human and rodent cardiomyopathy and aortopathy

We first screened failing human hearts (3,4) and human aortic aneurysm samples (14) and found both tissues to be markedly deficient in *Klf15* messenger RNA (mRNA) (Fig. 1, A and B). *Klf15* is a zinc finger transcription factor expressed in cardiomyocytes and cardiac fibroblasts that can repress hypertrophic signaling (15,16). Although it is also expressed in vascular smooth muscle cells (SMCs) (17), its role in vascular biology is unknown. We therefore hypothesized that *Klf15* mRNA deficiency might be common to the pathogenesis of both cardiomyopathy and aortopathy. We first confirmed that *Klf15* mRNA concentrations were also reduced in mice by using a well-established angiotensin II (AngII) infusion model to simultaneously stress the heart and vasculature (fig. S1, A and B) (8,18,19). Chronic AngII stimulation reduced *Klf15* mRNA expression in the heart and aorta of mice in vivo (Fig. 1, C and D) and in cultured cardiomyocytes and vascular SMCs (fig. S1C). *Klf15* mRNA concentrations were also reduced in another model of AngII-mediated cardiomyopathy in which the angiotensin type I receptor (AT1R) is overexpressed in a cardiac-specific fashion (20) (Fig. 1E). Together, these data demonstrate that *Klf15* mRNA

expression is significantly reduced in both human and rodent cardiomyopathy and aortopathy.

Klf15 deficiency causes severe cardiomyopathy and aortopathy

Given this expression pattern, we hypothesized that Klf15 deficiency might cause cardiomyopathy and aortopathy. To test this hypothesis, we studied mice with germline deficiency of *Klf15* (15) at baseline and after chronic AngII infusion. At baseline, *Klf15*$^{-/-}$ mice have mild pathologic remodeling of the heart [mild left ventricular (LV) hypertrophy with preserved systolic function; fig. S2, A to D, and table S1] and aorta (mild medial hypertrophy; fig. S2E). However, after AngII infusion, *Klf15*$^{-/-}$ mice develop a severe cardiomyopathy characterized by cardiomegaly, LV dysfunction, and cavity dilation with attenuated wall thickening (Fig. 2, A to C, and table S2). These pathologic changes were associated with augmented cardiac mass (fig. S3A). This phenotype was not due to differential blood pressure responses between wild-type and *Klf15*$^{-/-}$ mice (fig. S3B).

The aorta of *Klf15*$^{-/-}$ mice was also more sensitive to AngII than those of control mice. Thirty-five percent of *Klf15*$^{-/-}$ mice developed grossly visible aortic aneurysms (72% abdominal aorta, 28% thoracic aorta), whereas no aneurysms were observed in wild-type controls ($P = 0.0003$, $n = 31$ per group) (Fig. 2D). A subset of these aneurysmal segments had intramural hematoma formation confirmed by histologic examination (Fig. 2E). No intramural hematoma or dissections were seen in wild-type aortas. The non-aneurysmal portions of *Klf15*$^{-/-}$ aortas also had diffuse abnormalities, many of which have also been seen in the pathogenesis of AngII-induced aortopathy (19,21,22). We observed a severe disruption of medial architecture characterized by prominent elastolysis (Fig. 2F), increased SMC apoptosis (fig. S4, A and B), and reduced medial thickness (Fig. 2G). In the tunica adventitia, *Klf15*$^{-/-}$ mice showed a blunted adventitial growth response to AngII (fig. S4C). These medial and adventitial abnormalities were associated with generalized aortic dilation (Fig. 2G). In addition, the SMC of *Klf15*$^{-/-}$ mice elaborated excessive matrix metalloproteinase-3 (MMP-3) (fig. S5, A and B), an enzyme implicated in aneurysm formation (23). Together, these data demonstrate that *Klf15*$^{-/-}$ aortas are highly sensitive to AngII and develop a diffuse aortopathy involving the tunica media and adventitia, with significantly increased frequency of aneurysm and intramural hematoma formation.

p53 is activated in the heart and aorta of *Klf15*$^{-/-}$ mice

Given the parallel phenotypes of organ decompensation in the heart and aorta in *Klf15*$^{-/-}$ mice, we hypothesized that *Klf15* deficiency may cause common signaling perturbations in both tissues. We focused attention on p53 as it is activated with AngII stimulation (24), plays a critical role in cardiac decompensation (18), and has been associated with aneurysm pathogenesis (6). Analysis of mouse heart and aortic tissue revealed a substantial accumulation of p53 in *Klf15*$^{-/-}$ mice after AngII infusion (Fig. 3, A and B). In addition, direct targets of p53, such as the proapoptotic protein Bax and the potent antiangiogenic and proapoptotic factor thrombospondin-1 (TSP-1) (25), were also significantly elevated in both the heart and the aorta (Fig. 3, A and C). The increase in TSP-1 was predominantly seen in the tunica adventitia and is consistent with our finding that adventitial growth is blunted in *Klf15*$^{-/-}$ aortas after AngII infusion. There was no significant difference in *p53* mRNA concentrations in these tissues (fig. S6, A and B), suggesting that its accumulation was a result of posttranslational regulation. Consistent with this in vivo data, KLF15 overexpression in cultured cardiomyocytes potently inhibited basal and AngII-mediated induction of TSP-1 (Fig. 3D), suggesting that KLF15 may inhibit expression of important p53 transcriptional targets. Because p53 accumulation in the heart is causally implicated in the transition from compensated hypertrophy to heart failure through its ability to inhibit myocardial angiogenesis (18), we quantified myocardial capillary density. AngII increases

capillary density in wild-type hearts by 30%, whereas it has no angiogenic effect in *Klf15*$^{-/-}$ hearts (Fig. 3E). The diffuse vessel dilation and blunted medial thickening in *Klf15*$^{-/-}$ aortas after AngII stimulation were also associated with a paucity of adventitial angiogenesis (Fig. 3F).

Germline deficiency of *p53* rescues heart failure and aortopathy in *Klf15*$^{-/-}$ mice

To establish a causal role for p53 in the cardiomyopathy and aortopathy of *Klf15*$^{-/-}$ mice, we backcrossed into the *p53*$^{-/-}$ strain (18,26) and assessed for rescue. *Klf15*$^{-/-}$ *p53*$^{-/-}$ mice were born in Mendelian ratios and viable into adulthood. As hypothesized, *p53* deficiency rescued AngII-induced systolic dysfunction, chamber dilation, and wall thinning in *Klf15*$^{-/-}$ hearts (Fig. 4, A and B). *p53* deficiency also ameliorated the aortopathy in *Klf15*$^{-/-}$ mice as evidenced by improved medial integrity (Fig. 4C). Furthermore, the p53-dependent rescue of these pathologic abnormalities was associated with attenuation of TSP-1 abundance (Fig. 4D). There was also rescue of the angiogenic defect in *Klf15*$^{-/-}$ hearts, with a significant augmentation of myocardial capillary density in *Klf15*$^{-/-}$ *p53*$^{-/-}$ relative to *Klf15*$^{-/-}$ *p53*$^{+/+}$ mice (Fig. 4E). *p53* deficiency had no differential effect on cardiac mass, consistent with its promotion of myocardial angiogenesis and compensated cardiac growth (18) (table S3). Consistentwith the antiangiogenic role of p53 in the heart (18), endothelial staining of aortic sections revealed that *p53* deficiency normalized capillary density and adventitial growth in *Klf15*$^{-/-}$ mice (Fig. 4F).

Klf15 inhibits p53 acetylation

We next explored how KLF15 might regulate p53 function. In *Klf15*$^{-/-}$ tissues, the increased abundance of p53 protein occurs in the absence of *p53* mRNA accumulation (Fig. 3, A and B, and fig. S6). Because p53 function is tightly controlled by an intricate network of posttranslational modifications and protein interactions (27, 28), we reasoned that KLF15 might alter this aspect of p53 regulation. KLF15 overexpression did not induce Mdm2 or Stub1 (two E3 ubiquitin ligases that can inactivate p53) (27, 29) in cultured cells, and neither protein was reduced in *Klf15*$^{-/-}$ hearts. KLF15 overexpression in cultured cardiomyocytes caused an attenuation of basal and AngII-induced p53 acetylation on Lys^{379} (equivalent to Lys^{382} in humans) (Fig. 5A), a residue that is specifically modified by the acetyltransferase p300 (28). KLF15 overexpression did not alter phosphorylation of p53 at Ser^{15}, a modification also important for p53 activation (27) (Fig. 5A). Consistent with our overexpression data, *Klf15*$^{-/-}$ hearts (Fig. 5B) and aortic SMCs (Fig. 5C) had significantly augmented abundance of acetylated p53 (Lys^{379}). Finally, we found that substantial p53 hyperacetylation also occurs in human disease, as failing human hearts showed an increased abundance of acetylated p53 (Lys^{382}) (Fig. 5D).

The acetyltransferase p300 is an important regulator of p53 function via its ability to acetylate p53 at multiple lysine residues, a modification critical for p53 transcriptional activity and protein stability (27,28). We reasoned that the KLF15-mediated inhibition of p53 acetylation might reflect its ability to disrupt p300 function. However, KLF15 overexpression did not reduce p300 abundance or acetyltransferase activity in cultured cardiomyocytes. Furthermore, there was only a modest effect on nuclear p300 accumulation in *Klf15*$^{-/-}$ hearts (fig. S7A) or in failing human hearts (Fig. 5D).

Pharmacologic inhibition of p300 rescues heart failure and aortopathy in *Klf15*$^{-/-}$ mice

Previous studies demonstrate a causal role for excessive p300 activity in heart failure (30,31), whereas its role in aortopathy is unknown. We hypothesized that when *Klf15* is deficient, p53 hyperacetylation reflects an enhanced state of p300 function that leads to cardiovascular decompensation. As such, targeting p300 function might rescue the cardiomyopathy and aortopathy observed in *Klf15*-deficient mice. Because germline

deficiency of *p300* results in early embryonic lethality (32), we tested this hypothesis by using the drug curcumin, a potent p300 acetyltransferase inhibitor (31,33). Mice were pretreated with curcumin for 7 days, followed by a 14-day AngII infusion with continued curcumin therapy (fig. S7B). Curcumin significantly ameliorated decompensated heart failure in *Klf15*$^{-/-}$ mice, with a reduction in cardiac mass (Fig. 6, A and B), improvement in LV systolic function (Fig. 6, C and D), attenuation of eccentric remodeling (Fig. 6, C and D, and table S4), and decrease in acetylated p53 abundance in tissues (Fig. 6E). Finally, we examined the aorta to assess whether curcumin could also rescue the aortopathy in *Klf15*$^{-/-}$ mice and found that curcumin caused a near normalization of elastolysis (Fig. 6F) and restoration of medial thickness (fig. S7C) without any significant effect on mean vessel diameter (fig. S7C).

DISCUSSION

Our central finding is that deficiency of the transcriptional regulator *Klf15* leads to cardiomyopathy and aortopathy via a shared mechanism in which there is derepression of p53 and p300 acetyltransferase. We further demonstrate that, in the setting of *Klf15* deficiency in mice, inhibition of this pathway can normalize these abnormalities in vivo. These conclusions are based on several observations. We first show that *Klf15* expression is reduced in both human and murine cardiomyopathy and aortopathy. *Klf15* deficiency can result in these disease phenotypes, as *Klf15*$^{-/-}$ mice develop severe heart failure and aortopathy in response to stress. KLF15 inhibits p53 function by reducing abundance of acetylated p53. Conversely, *Klf15* deficiency leads to p53 hyperacetylation and enhanced p53 effector functions, findings that are recapitulated in human disease. A causal role for this pathway is established by the observation that both genetic ablation of *p53* and pharmacologic inhibition of p300 acetyltransferase with curcumin can both ameliorate the cardiovascular abnormalities seen in *Klf15*$^{-/-}$ mice. Thus, deficiency of a single transcription factor can exert detrimental effects in the heart and vasculature through a unifying molecular mechanism.

On the basis of these observations, we propose the model shown in Fig. 6G. Pathologic stressors such as AngII down-regulate KLF15 and promote p53 accumulation (24). Excessive p53 accumulation leads to diminished angiogenesis, apoptotic cell loss, decompensated heart failure (18,24), and aneurysmal aortopathy. These diseases are accelerated in *Klf15*$^{-/-}$ mice in a p53-dependent manner. KLF15 can inhibit p53 function via interfering with p300-mediated acetylation. As such, we propose that KLF15 is a molecular brake on p53 and that genetic deficiency of *Klf15* leads to unbridled p53 activity in response to stress. The partial reduction of KLF15 concentrations in the heart and aorta in response to AngII might represent a molecular program that initially facilitates compensated forms of tissue remodeling. However, sustained reduction of KLF15 or its complete absence may sensitize both tissues to grossly decompensate in response stress. The fact that excessive p300 acetyltransferase activity also contributes to this phenotype implicates hyperacetylation of p53 as a critical component of this maladaptive signaling pathway. We recognize, however, that p300 can acetylate other factors that have important roles in pathologic cardiovascular remodeling, such as GATA4, MEF2, histones, and Smad (30,31,34). Indeed, KLF15 might also disrupt the ability of p300 to acetylate and coactivate these factors, suggesting how it might exert its potent repressive effect on multiple transcriptional pathways (2,15). In addition to its ability to disrupt p300-mediated acetylation of p53, KLF15 might simultaneously facilitate the ability of p53 to interact with deacetylases (27) or other inhibitory proteins (27,35). Such possibilities are consistent with our model and may contribute to selective regulation of p53 effector functions (27).

Recent studies have elegantly elucidated an intricate network of AngII–TGF-β (transforming growth factor–β) cross talk that is central to the pathogenesis of heart failure (36) and aortopathy (5,37,38). Our model has numerous points of intersection with the TGF-β signaling pathway. We show that *Klf15*$^{-/-}$ mice have exaggerated expression of TSP-1, a well-characterized transcriptional target of p53 (25,39) that is an endogenous activator of latent TGF-β (40) and one of the most potent antiangiogenic proteins in mammalian biology (41). The observation that *p53* deficiency attenuates TSP-1 concentrations in tissues of *Klf15*$^{-/-}$ mice confirms that its maximal induction is p53-dependent in vivo. Because p53-mediated inhibition of angiogenesis causes cardiac decompensation (18), TSP-1 might be an important downstream mediator of this effect. Although the role of angiogenesis in aortic disease is less well established, we find that the aortopathy in *Klf15*$^{-/-}$ mice is associated with a p53-dependent attenuation of adventitial angiogenesis. These observations raise the possibility that localized angiogenic insufficiency in the tunica adventitia might contribute to aortopathy and are consistent with a recent study implicating pathologic changes in the adventitia as contributors to the progression of aortic disease (22). In addition to its antiangiogenic capabilities, TSP-1 can markedly potentiate TGF-β signaling at the cell surface by its ability to activate latent TGF-β (40). The final point of intersection between the two pathways is in the nucleus, where p300 and p53 can both cooperate with Smads and potentiate Smad-mediated transcription (42). Definition of the role of *Klf15* as a regulator of the AngII–TGF-β axis in vivo may provide insight into the pathogenesis of Marfan's disease and related disorders (5,7,38).

The current study extends our previous observations (15,16) and implicates *Klf15* as a central regulator of stress responses in both the heart and the vasculature. In addition, we identify the *Klf15*$^{-/-}$ mouse as a model for aortic aneurysm formation in which lesions develop at modest AngII doses without requiring an *ApoE*$^{-/-}$ background (19). On the basis of our observations in humans and rodents, we propose that a subset of human heart and vascular disease may be due to KLF15 deficiency and that the *Klf15-p53-p300* pathway is a potential therapeutic target for cardiovascular disease.

MATERIALS AND METHODS

Animal models

All protocols concerning animal use were approved by the Institutional Animal Care and Use Committee at Case Western Reserve University and conducted in accordance with the National Institutes of Health *Guide for the Care and Use of Laboratory Animals*. *Klf15*$^{-/-}$ mice (15) (10 weeks old, male) and littermate controls in a pure C57Bl/6 background were used for all studies. *p53*$^{-/-}$ mice (18,26) were from The Jackson Laboratory. For infusion studies, mice were anesthetized with ketamine (1.5 mg per kilogram of body weight)–xylazine (0.3 mg/kg). Mini-osmotic pumps (Alzet 2002, Durect) were filled with AngII (Sigma) or vehicle (normal saline) and implanted subcutaneously. AngII was infused at a dose of 1.4 mg/kg per day for 14 days, after which mice were killed for further analysis. Curcumin (Sigma) was freshly suspended in 0.5% carboxymethylcellulose (Sigma) and administered to mice via oral gavage at a dose of 100 mg/kg per day divided into two daily doses. For perfusion fixation, the thorax was opened, a 21-gauge needle was placed into the left ventricle, and the inferior vena cava was severed. The animals were perfused with normal saline until the perfusate cleared and then with 4% paraformaldehyde at 100 mmHg for 7 min. RNA samples from *AT1R*-transgenic and nontransgenic mice were gifts from J. Sadoshima (20).

Echocardiographic and blood pressure analysis

For transthoracic echocardiography, mice were anesthetized with 1% inhalational isoflurane and imaged using the Vevo 770 High Resolution Imaging System (Visual Sonics) and the RMV-707B 30-MHz probe. Measurements were obtained from M-mode sampling and from integrated EKV images that were taken in the LV short axis at the midpapillary level (15). Conscious systolic blood pressure was measured using the BP2000 Blood Pressure Analysis System (Visitech Systems) as recommended by the manufacturer. To allow mice to adapt to the apparatus, we performed daily blood pressure measurements for 1 week before beginning experiments. Blood pressure was recorded at days 0 and 14 of the infusions.

Human samples

LV samples from nonfailing control (n = 30) and nonischemic cardiomyopathy (NICM) (n = 36) subjects were obtained as described (3,4) in accordance with the Investigation Review Committee at the Hospital of the University of Pennsylvania (Philadelphia, PA). Aneurysmal tissue was collected from patients undergoing abdominal aortic aneurysm repair operations as described (14). Control abdominal aortic specimens were matched to cases using sex, age, and ethnicity as described (14). All aortic specimens were obtained by protocols approved by the Institutional Review Board of Wayne State University (Detroit, MI). RNA was isolated from each sample as described (3,4,14). Taqman quantitative polymerase chain reaction (QPCR) was used to quantify expression of *Klf15* with Applied Biosystems Assays-on-Demand Hs00362736_m1 using the $\Delta\Delta C_t$ method as described (3,4).

Tissue culture and adenoviral infection

Neonatal rat ventricular myocytes (NRVMs) were isolated from the hearts of rat pups as described (15). Primary mouse aortic SMCs (MASMCs) were cultured from aortas of wild-type and *Klf15*$^{-/-}$ mice as described (43). Rat aortic SMCs (RASMCs; used at passages 3 to 7), human embryonic kidney 293, and HCT116 cells were obtained from the American Type Culture Collection. NRVMs and RASMCs were placed in serum-free medium before stimulation with AngII (1 μM). Adenovirus (Ad-GFP versus Ad-KLF15-GFP) has been described (15). NRVMs were infected at 50 multiplicities of infection (MOIs) for 24 hours and RASMCs at 100 MOIs for 24 hours.

Histone acetyltransferase assays

Immunoprecipitation histone acetyltransferase (HAT) assays were performed using the p300 IP HAT Assay kit (Upstate-Millipore) according to the manufacturer's instructions.

RNA analysis from cells and animal samples

Total RNA was isolated from cells or tissues using Trizol (Invitrogen). Northern blot analysis for *Klf15* was performed as described (15). For QPCR, total RNA was deoxyribonuclease-treated (Invitrogen) and transcribed to complementary DNA with oligo(dT) or random hexamer priming (Invitrogen) and Moloney murine leukemia virus reverse transcriptase (New England Biolabs). QPCR was performed with the SYBR Green method on a Stratagene Mx3005P system. Relative expression was calculated using the $\Delta\Delta C_t$ method with normalization to constitutive genes as indicated in the figure legends. Specific primer sequences are available on request.

Western blot analysis

Total cellular or tissue homogenates were processed in radioimmunoprecipitation assay buffer (Sigma) supplemented with protease or phosphatase inhibitors (Roche). Nuclear protein was isolated using a Nuclear Extraction kit (NE-Per kit, Pierce) according to the manufacturer's instructions. Ten to 40 μg of whole protein extracts or 20 μg of nuclear

extracts was subjected to Western blot analysis. Antibodies against p53 (DO-1), p300 (N-15), β-actin (AC-15), myc (9E10), and Ku70 (E-5) were from Santa Cruz Biotechnology. Antibodies against acetyl p53 (Lys^{379} and Lys^{382}), phospho-p53 (Ser^{15}), and Bax were from Cell Signaling Technology. Antibody against TSP-1 (Ab4, clone A6.1) was from NeoMarkers–Thermo Fisher Scientific. Antibodies against glyceraldehyde-3-phosphate dehydrogenase (GAPDH) and FLAG (M2) were from Sigma. Antibody against Mdm2 (Ab-3, clone 4B11) was from Calbiochem–EMD Biosciences. Stub1 polyclonal antibody serum was a gift from C. Patterson (University of North Carolina, Chapel Hill, NC) (29).

Protein secretion from cultured SMCs

Primary MASMCs were serum starved for 24 hours, followed by stimulation with AngII (1 μM, 6 hours). Supernatants were subjected to enzyme-linked immunosorbent assay (ELISA) for MMP-3 using the SearchLight Proteome Array or multiplex sandwich ELISA (Pierce Biotechnology).

Histologic and morphometric analysis

Perfusion-fixed ventricles and aortas were embedded in paraffin and cut into 5-μm-thick sections. Medial thickness and area were quantified using Image-Pro Plus software (Media Cybernetics). Trichrome staining of heart tissue was performed using the One-Step Trichrome kit (Biocare Medical) according to the manufacturer's instructions. Elastin staining of aortic sections was performed on perfusion-fixed aortic cross sections (5 μm thick) using Elastin Stain kit (Sigma) according to the manufacturer's instructions. Quantification of elastin degradation was a direct adaptation of the semiquantitative aortic wall architecture score (5). An elastin break was defined as a distinct discontinuity in a singular concentric lamellar ring of elastin. The total number of elastin breaks in a vessel cross section was counted as a single data point. The aortic sections being compared were from the same aortic level for each mouse. Measurements were performed by two independent and blinded observers. Vessel diameter was quantified from elastin-stained circular aortic sections. We defined diameter as the mean distance between internal elastic laminae on diametrically opposite sides of the vessel ring. TSP-1 immunostaining was performed using antibody against TSP-1 (Ab4, clone A6.1). Antibody against MMP-3 for immunostaining was from Abcam. To assess capillary density in aortic cross sections, we performed CD34 antibody immunofluorescence staining (Chemicon) on fresh-frozen aortic sections using Alexa Fluor 488–labeled secondary antibody and 4′,6-diamidino-2-phenylindole (DAPI) counterstaining. All comparisons were made between sections cut from the same aortic level.

Terminal deoxynucleotidyl transferase–mediated deoxyuridine triphosphate nick end labeling staining

Terminal deoxynucleotidyl transferase–mediated deoxyuridine triphosphate nick end labeling (TUNEL) staining was performed on perfusion-fixed sections (8 μm thick) of heart and aortas using the ApopTag Plus kit (Chemicon) according to the manufacturer's instructions. MASMCs were stimulated with AngII (1 μM) for 72 hours and assessed for TUNEL using the *In Situ* Cell Death Detection kit (Roche) according to the manufacturer's instructions. DAPI counterstaining and mounting was done with Vectashield H-1500 mounting medium (Vector Labs). TUNEL-positive nuclei per section were normalized to total nuclei using Image-Pro Plus software.

Analysis of myocardial capillary density

Fresh-frozen sections of mouse LV were cut into 8-μm-thick sections, fixed in 100% ethanol, and dual-stained for platelet endothelial cell adhesion molecule–1 (PECAM-1) and

wheat germ agglutinin (WGA) as described (18,44). Antibody against PECAM-1 was from Millipore and used at 1:100 dilution. Secondary antibody (antibody against rat immunoglobulin labeled with Alexa Fluor 488) was from Invitrogen and used at 1:800 dilution. WGA-rhodamine (5 μg/ml; Vector Labs) counterstaining was applied after immunostaining. Random high-power fields (HPFs) (400×) were imaged using a fluorescent microscope. Intramyocardial capillaries and myocytes were counted and quantified as described (18,44).

Statistical analysis

All data are presented as the mean ± SEM. For continuous variables, the statistical significance of differences between two groups was analyzed with two-tailed unpaired Student's *t* test. The statistical significance for the frequency of occurrence of a binary variable (that is, presence or absence of aortic aneurysm) was analyzed using χ^2 test of association and two-tailed Fisher's exact probability test. Values of $P < 0.05$ were considered significant.

Supplementary Material

Refer to Web version on PubMed Central for supplementary material.

REFERENCES AND NOTES

1. Heineke J, Molkentin JD. Regulation of cardiac hypertrophy by intracellular signalling pathways. Nat. Rev. Mol. Cell Biol 2006;7:589–600. [PubMed: 16936699]
2. Haldar SM, Ibrahim OA, Jain MK. Kruppel-like factors (KLFs) in muscle biology. J. Mol. Cell. Cardiol 2007;43:1–10. [PubMed: 17531262]
3. Hannenhalli S, Putt ME, Gilmore JM, Wang J, Parmacek MS, Epstein JA, Morrisey EE, Margulies KB, Cappola TP. Transcriptional genomics associates FOX transcription factors with human heart failure. Circulation 2006;114:1269–1276. [PubMed: 16952980]
4. Margulies KB, Matiwala S, Cornejo C, Olsen H, Craven WA, Bednarik D. Mixed messages: Transcription patterns in failing and recovering human myocardium. Circ. Res 2005;96:592–599. [PubMed: 15718504]
5. Habashi JP, Judge DP, Holm TM, Cohn RD, Loeys BL, Cooper TK, Myers L, Klein EC, Liu G, Calvi C, Podowski M, Neptune ER, Halushka MK, Bedja D, Gabrielson K, Rifkin DB, Carta L, Ramirez F, Huso DL, Dietz HC. Losartan, an AT1 antagonist, prevents aortic aneurysm in a mouse model of Marfan syndrome. Science 2006;312:117–121. [PubMed: 16601194]
6. Ihling C, Szombathy T, Nampoothiri K, Haendeler J, Beyersdorf F, Uhl M, Zeiher AM, Schaefer HE. Cystic medial degeneration of the aorta is associated with p53 accumulation, Bax upregulation, apoptotic cell death, and cell proliferation. Heart 1999;82:286–293. [PubMed: 10455077]
7. Judge DP, Dietz HC. Marfan's syndrome. Lancet 2005;366:1965–1976. [PubMed: 16325700]
8. Shindo T, Manabe I, Fukushima Y, Tobe K, Aizawa K, Miyamoto S, Kawai-Kowase K, Moriyama N, Imai Y, Kawakami H, Nishimatsu H, Ishikawa T, Suzuki T, Morita H, Maemura K, Sata M, Hirata Y, Komukai M, Kagechika H, Kadowaki T, Kurabayashi M, Nagai R. Krüppel-like zinc-finger transcription factor KLF5/BTEB2 is a target for angiotensin II signaling and an essential regulator of cardiovascular remodeling. Nat. Med 2002;8:856–863. [PubMed: 12101409]
9. Lin AE, Basson CT, Goldmuntz E, Magoulas PL, McDermott DA, McDonald-McGinn DM, McPherson E, Morris CA, Noonan J, Nowak C, Pierpont ME, Pyeritz RE, Rope AF, Zackai E, Pober BR. Adults with genetic syndromes and cardiovascular abnormalities: Clinical history and management. Genet. Med 2008;10:469–494. [PubMed: 18580689]
10. van der Klaauw AA, Bax JJ, Smit JW, Holman ER, Delgado V, Bleeker GB, Biermasz NR, Roelfsema F, Romijn JA, Pereira AM. Increased aortic root diameters in patients with acromegaly. Eur. J. Endocrinol 2008;159:97–103. [PubMed: 18495693]

11. Lakatta EG. Arterial and cardiac aging: Major shareholders in cardiovascular disease enterprises. Part III: Cellular and molecular clues to heart and arterial aging. Circulation 2003;107:490–497. [PubMed: 12551876]
12. Jessup M, Brozena S. Heart failure. N. Engl. J. Med 2003;348:2007–2018. [PubMed: 12748317]
13. Cannon CP, Braunwald E, McCabe CH, Rader DJ, Rouleau JL, Belder R, Joyal SV, Hill KA, Pfeffer MA, Skene AM. Pravastatin or Atorvastatin Evaluation and Infection Therapy-Thrombolysis in Myocardial Infarction 22 Investigators, Intensive versus moderate lipid lowering with statins after acute coronary syndromes. N. Engl. J. Med 2004;350:1495–1504. [PubMed: 15007110]
14. Lenk GM, Tromp G, Weinsheimer S, Gatalica Z, Berguer R, Kuivaniemi H. Whole genome expression profiling reveals a significant role for immune function in human abdominal aortic aneurysms. BMC Genomics 2007;8:237. [PubMed: 17634102]
15. Fisch S, Gray S, Heymans S, Haldar SM, Wang B, Pfister O, Cui L, Kumar A, Lin Z, Sen-Banerjee S, Das H, Petersen CA, Mende U, Burleigh BA, Zhu Y, Pinto YM, Liao R, Jain MK. Kruppel-like factor 15 is a regulator of cardiomyocyte hypertrophy. Proc. Natl. Acad. Sci. U.S.A 2007;104:7074–7079. [PubMed: 17438289]
16. Wang B, Haldar SM, Lu Y, Ibrahim OA, Fisch S, Gray S, Leask A, Jain MK. The Kruppellike factor KLF15 inhibits connective tissue growth factor (CTGF) expression in cardiac fibroblasts. J. Mol. Cell. Cardiol 2008;45:193–197. [PubMed: 18586263]
17. Gray S, Feinberg MW, Hull S, Kuo CT, Watanabe M, Sen-Banerjee S, DePina A, Haspel R, Jain MK. The Krüppel-like factor KLF15 regulates the insulin-sensitive glucose transporter GLUT4. J. Biol. Chem 2002;277:34322–34328. [PubMed: 12097321]
18. Sano M, Minamino T, Toko H, Miyauchi H, Orimo M, Qin Y, Akazawa H, Tateno K, Kayama Y, Harada M, Shimizu I, Asahara T, Hamada H, Tomita S, Molkentin JD, Zou Y, Komuro I. p53-induced inhibition of Hif-1 causes cardiac dysfunction during pressure overload. Nature 2007;446:444–448. [PubMed: 17334357]
19. Daugherty A, Manning MW, Cassis LA. Angiotensin II promotes atherosclerotic lesions and aneurysms in apolipoprotein E–deficient mice. J. Clin. Invest 2000;105:1605–1612. [PubMed: 10841519]
20. Zhai P, Yamamoto M, Galeotti J, Liu J, Masurekar M, Thaisz J, Irie K, Holle E, Yu X, Kupershmidt S, Roden DM, Wagner T, Yatani A, Vatner DE, Vatner SF, Sadoshima J. Cardiac-specific overexpression of AT1 receptor mutant lacking Gαq/Gαi coupling causes hypertrophy and bradycardia in transgenic mice. J. Clin. Invest 2005;115:3045–3056. [PubMed: 16276415]
21. Henderson EL, Geng YJ, Sukhova GK, Whittemore AD, Knox J, Libby P. Death of smooth muscle cells and expression of mediators of apoptosis by T lymphocytes in human abdominal aortic aneurysms. Circulation 1999;99:96–104. [PubMed: 9884385]
22. Tieu BC, Lee C, Sun H, Lejeune W, Recinos A III, Ju X, Spratt H, Guo DC, Milewicz D, Tilton RG, Brasier AR. An adventitial IL-6/MCP1 amplification loop accelerates macrophage-mediated vascular inflammation leading to aortic dissection in mice. J. Clin. Invest 2009;119:3637–3651. [PubMed: 19920349]
23. Silence J, Lupu F, Collen D, Lijnen HR. Persistence of atherosclerotic plaque but reduced aneurysm formation in mice with stromelysin-1 (MMP-3) gene inactivation. Arterioscler. Thromb. Vasc. Biol 2001;21:1440–1445. [PubMed: 11557669]
24. Leri A, Claudio PP, Li Q, Wang X, Reiss K, Wang S, Malhotra A, Kajstura J, Anversa P. Stretch-mediated release of angiotensin II induces myocyte apoptosis by activating p53 that enhances the local renin-angiotensin system and decreases the Bcl-2-to-Bax protein ratio in the cell. J. Clin. Invest 1998;101:1326–1342. [PubMed: 9525975]
25. Dameron KM, Volpert OV, Tainsky MA, Bouck N. Control of angiogenesis in fibroblasts by p53 regulation of thrombospondin-1. Science 1994;265:1582–1584. [PubMed: 7521539]
26. Jacks T, Remington L, Williams BO, Schmitt EM, Halachmi S, Bronson RT, Weinberg RA. Tumor spectrum analysis in p53-mutant mice. Curr. Biol 1994;4:1–7. [PubMed: 7922305]
27. Kruse JP, Gu W. Modes of p53 regulation. Cell 2009;137:609–622. [PubMed: 19450511]
28. Tang Y, Zhao W, Chen Y, Zhao Y, Gu W. Acetylation is indispensable for p53 activation. Cell 2008;133:612–626. [PubMed: 18485870]

29. Qian SB, McDonough H, Boellmann F, Cyr DM, Patterson C. CHIP-mediated stress recovery by sequential ubiquitination of substrates and Hsp70. Nature 2006;440:551–555. [PubMed: 16554822]

30. Wei JQ, Shehadeh LA, Mitrani JM, Pessanha M, Slepak TI, Webster KA, Bishopric NH. Quantitative control of adaptive cardiac hypertrophy by acetyltransferase p300. Circulation 2008;118:934–946. [PubMed: 18697823]

31. Morimoto T, Sunagawa Y, Kawamura T, Takaya T, Wada H, Nagasawa A, Komeda M, Fujita M, Shimatsu A, Kita T, Hasegawa K. The dietary compound curcumin inhibits p300 histone acetyltransferase activity and prevents heart failure in rats. J. Clin. Invest 2008;118:868–878. [PubMed: 18292809]

32. Yao TP, Oh SP, Fuchs M, Zhou ND, Ch'ng LE, Newsome D, Bronson RT, Li E, Livingston DM, Eckner R. Gene dosage-dependent embryonic development and proliferation defects in mice lacking the transcriptional integrator p300. Cell 1998;93:361–372. [PubMed: 9590171]

33. Balasubramanyam K, Varier RA, Altaf M, Swaminathan V, Siddappa NB, Ranga U, Kundu TK. Curcumin, a novel p300/CREB-binding protein-specific inhibitor of acetyltransferase, represses the acetylation of histone/nonhistone proteins and histone acetyltransferase-dependent chromatin transcription. J. Biol. Chem 2004;279:51163–51171. [PubMed: 15383533]

34. Tu AW, Luo K. Acetylation of Smad2 by the co-activator p300 regulates activin and transforming growth factor β response. J. Biol. Chem 2007;282:21187–21196. [PubMed: 17478422]

35. Grönroos E, Terentiev AA, Punga T, Ericsson J. YY1 inhibits the activation of the p53 tumor suppressor in response to genotoxic stress. Proc. Natl. Acad. Sci. U.S.A 2004;101:12165–12170. [PubMed: 15295102]

36. Rosenkranz S. TGF-β1 and angiotensin networking in cardiac remodeling. Cardiovasc. Res 2004;63:423–432. [PubMed: 15276467]

37. Brooke BS, Habashi JP, Judge DP, Patel N, Loeys B, Dietz HC III. Angiotensin II blockade and aortic-root dilation in Marfan's syndrome. N. Engl. J. Med 2008;358:2787–2795. [PubMed: 18579813]

38. Loeys BL, Schwarze U, Holm T, Callewaert BL, Thomas GH, Pannu H, De Backer JF, Oswald GL, Symoens S, Manouvrier S, Roberts AE, Faravelli F, Greco MA, Pyeritz RE, Milewicz DM, Coucke PJ, Cameron DE, Braverman AC, Byers PH, De Paepe AM, Dietz HC. Aneurysm syndromes caused by mutations in the TGF-β receptor. N. Engl. J. Med 2006;355:788–798. [PubMed: 16928994]

39. Mirochnik Y, Kwiatek A, Volpert OV. Thrombospondin and apoptosis: Molecular mechanisms and use for design of complementation treatments. Curr. Drug Targets 2008;9:851–862. [PubMed: 18855619]

40. Schultz-Cherry S, Lawler J, Murphy-Ullrich JE. The type 1 repeats of thrombospondin 1 activate latent transforming growth factor-β. J. Biol. Chem 1994;269:26783–26788. [PubMed: 7929414]

41. Teodoro JG, Evans SK, Green MR. Inhibition of tumor angiogenesis by p53: A new role for the guardian of the genome. J. Mol. Med 2007;85:1175–1186. [PubMed: 17589818]

42. Atfi A, Baron R. p53 brings a new twist to the Smad signaling network. Sci. Signal 2008;1:pe33. [PubMed: 18594115]

43. Fritz KE, Jarmolych J, Daoud AS, Landau JV. Aortic explant culture: A versatile technique especially useful in studies of atherogenesis. Methods Cell Science 1978;4:863–866.

44. Heineke J, Auger-Messier M, Xu J, Oka T, Sargent MA, York A, Klevitsky R, Vaikunth S, Duncan SA, Aronow BJ, Robbins J, Crombleholme TM, Molkentin JD. Cardiomyocyte GATA4 functions as a stress-responsive regulator of angiogenesis in the murine heart. J. Clin. Invest 2007;117:3198–3210. [PubMed: 17975667]

45. **Acknowledgments:** We thank R. A. Walsh, D. I. Simon, and J. S. Stamler for critical review of the manuscript; J. Sadoshima for providing RNA samples from *AT1R*-transgenic mice; and C. Patterson for providing antibody against Stub1. **Funding:** NIH grants HL086614 (S.M.H.), HL072952 and HL084154 (M.K.J.), HL094660 (D.J.), and HL064310 (H.K.); American Heart Association Postdoctoral Fellowship (D.K.); American Society of Transplantation Faculty Development grant (K.S.); American Heart Association Scientist Development grant (K.S.); and Visconsi Research Scholars' Fund (S.M.H.). **Author contributions:** M.K.J. served as the

principal investigator. S.M.H., Y. Lu, and M.K.J. prepared the manuscript. S.M.H. and Y. Lu were responsible for design and execution of experiments, interpretation of results, and supervision of technical personnel. J.S. provided mouse heart RNA samples and provided critical data interpretation and manuscript review. K.B.M. and T.P.C. provided human myocardial samples, data interpretation, and critical manuscript review. Y. Li performed QPCR on human myocardial samples. H.K. and K.S. provided human aortic samples and critical manuscript review. D.J., D.K., S.J.E., and C.H. assisted with animal care, QPCR, Western blotting, and histology. Y.C. performed all animal surgeries. Y.-Q.D. and M.W. performed histopathologic analyses.
Competing interests: The authors declare no competing interests.

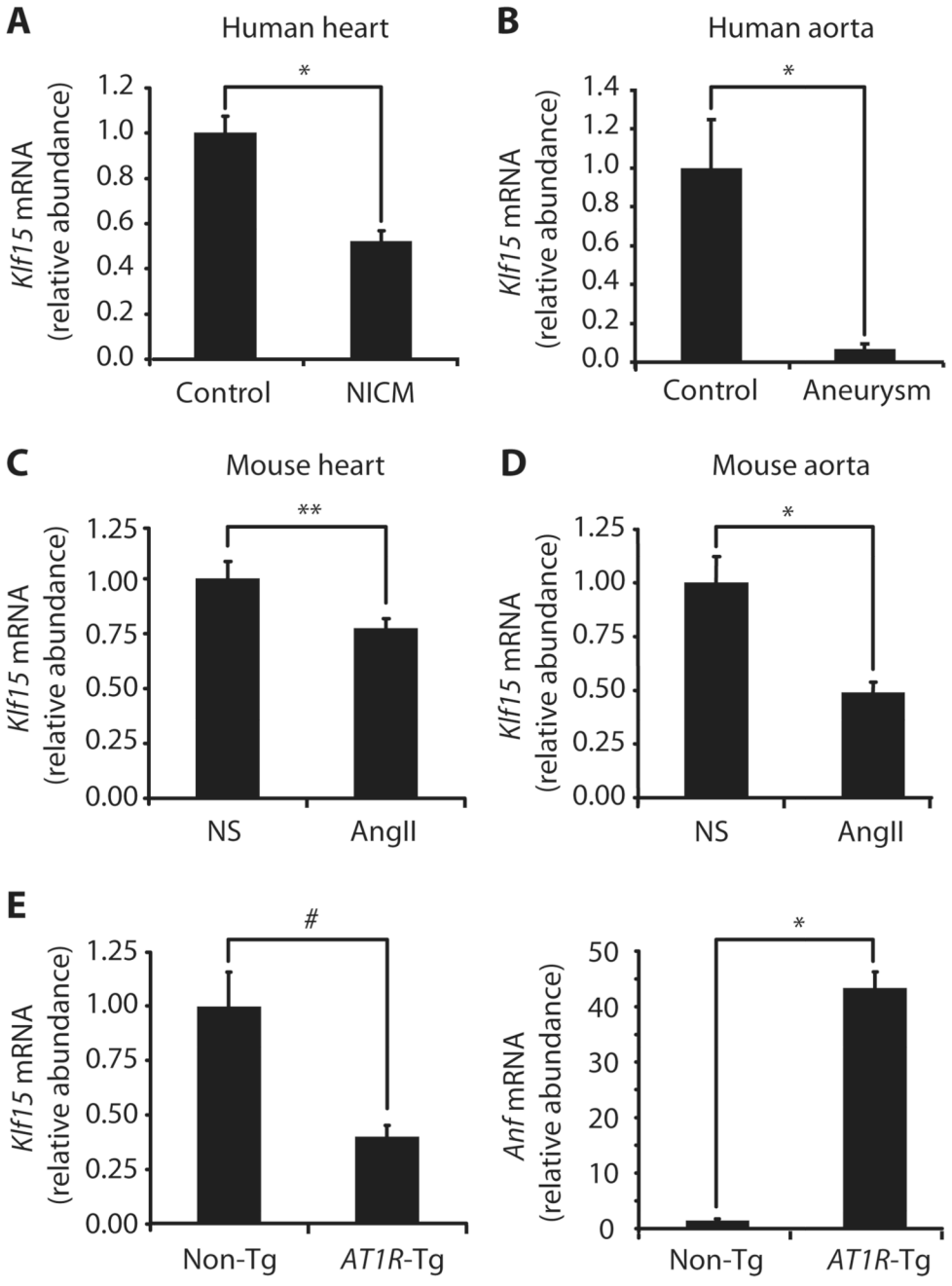

Fig. 1.

Klf15 concentration is reduced in cardiomyopathy and aortopathy in humans and rodents. (**A**) *Klf15* expression from LV samples of patients with non-ischemic cardiomyopathy (NICM) (*n* = 36) and controls (*n* = 30). Values normalized to *Gapdh*. (**B**) *Klf15* expression from aortic samples of patients with abdominal aortic aneurysms (*n* = 5) and control abdominal aortas (*n* = 7). Values normalized to *18S*. (**C**) Ventricular RNA from normal saline (NS)–infused (*n* = 7) or AngII-infused (*n* = 9) mice analyzed for *Klf15* expression. Values normalized to *cyclophilin B*. (**D**) Aortic RNA from normal saline–infused (*n* = 7) or AngII-infused (*n* = 9) mice analyzed for *Klf15* expression. Values normalized to *cyclophilin B*. (**E**) *Klf15* (left) and *Anf* (right) expression from hearts of *AT1R*-transgenic (*AT1R*-Tg)

mice ($n = 3$) and nontransgenic (Non-Tg) controls ($n = 3$). Values normalized to *Gapdh*. *$P < 0.001$, **$P < 0.05$, $^{\#}P < 0.02$.

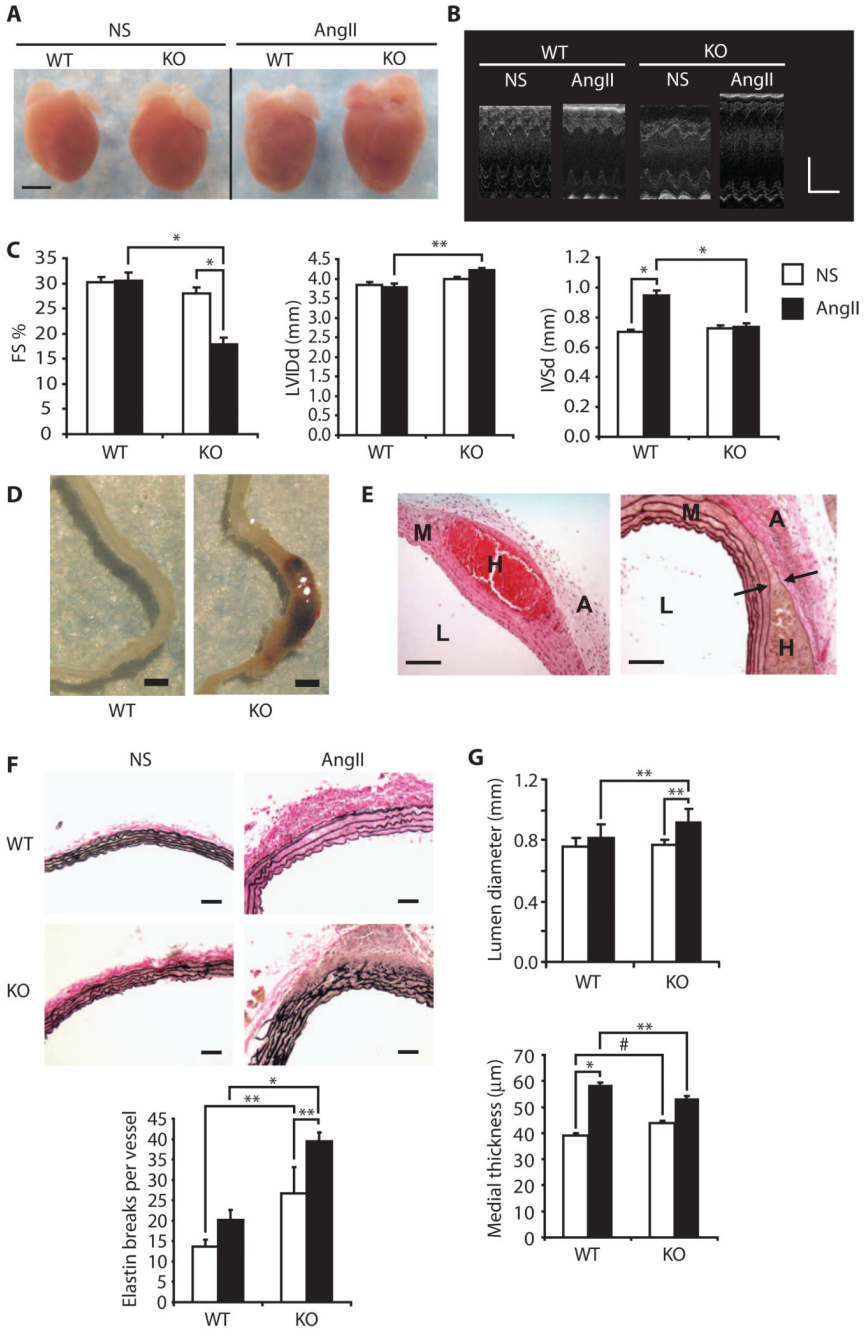

Fig. 2.

Klf15 deficiency leads to heart failure and aortic aneurysm formation. (**A**) Photographs of freshly excised hearts. Scale bar, 2.5 mm. (**B**) Representative M-mode echocardiographic images. Vertical scale bar, 2 mm; horizontal scale bar, 2 ms. (**C**) Fractional shortening (FS), LV diastolic diameter (LVIDd), and interventricular septal diastolic thickness (IVSd) in wild-type (WT) and $Klf15^{-/-}$ (KO) mice infused with normal saline ($n = 4$ per group) or AngII ($n = 5$ per group). $^{*}P < 0.001$, $^{**}P < 0.002$. (**D**) Representative photographs of freshly excised descending aortas from wild-type and $Klf15^{-/-}$ mice after AngII infusion. Scale bar, 2 mm. (**E**) Representative photomicrograph of intramural hematoma in AngII-infused $Klf15^{-/-}$ mice aorta. Left, hematoxylin and eosin staining; right, elastin staining.

Black arrows designate two distinct elastic laminae with enclosed hematoma. Scale bar, 50 μm. L, lumen; M, media; A, adventitia; H, hematoma. (**F**) Representative elastin-stained aortic sections from wild-type and *Klf15*$^{-/-}$ mice infused with normal saline (n = 4 per group) or AngII (n = 5 per group) with quantification of elastin degradation. Scale bar, 50 μm. *P < 0.001, **P < 0.05. (**G**) Quantitative morphometry (lumen diameter and medial thickness) of perfusion-fixed aortic cross sections from wild-type and *Klf15*$^{-/-}$ mice infused with normal saline (n = 6 per group) or AngII (n = 7 per group). *P < 0.001, **P < 0.05, $^{\#}P$ < 0.005.

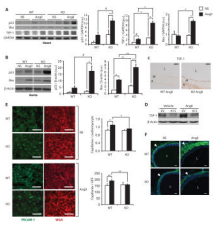

Fig. 3.

p53 is activated in the heart and aorta of *Klf15*$^{-/-}$ mice. (**A**) Western blot of p53, Bax, TSP-1, and GAPDH in whole-heart lysates from wild-type and *Klf15*$^{-/-}$ mice after normal saline or AngII infusion. Densitometric quantification to the right (normal saline, $n = 4$ per group; AngII, $n = 5$ per group). *$P < 0.001$, **$P < 0.05$, $^{\#}P < 0.02$. a.u., arbitrary units. (**B**) Western blot of p53, Bax, and β-actin in whole-aorta lysates from wild-type and *Klf15*$^{-/-}$ mice after normal saline or AngII infusion. Densitometric quantification to the right (normal saline, $n = 4$ per group; AngII, $n = 4$ per group). *$P < 0.01$, **$P < 0.05$, $^{\#}P < 0.03$. (**C**) TSP-1 antibody immunostaining of aortic cross sections from wild-type and *Klf15*$^{-/-}$ mice after AngII stimulation. (**D**) Western blot of TSP-1 and β-actin from neonatal rat ventricular myocytes infected with control virus (EV) or Ad-KLF15 (K15) and then stimulated with vehicle (PBS) or AngII. (**E**) Representative photomicrographs of LV cross sections from wild-type and *Klf15*$^{-/-}$ mice after normal saline or AngII infusion stained with antibody against PECAM-1 (green) to identify intramyocardial vessels and WGA-rhodamine (red) to outline cardiomyocytes. Quantification of capillary density normalized per cardiomyocyte (top) or per high-power field (HPF, bottom) ($n = 6$ per group). *$P < 0.01$, **$P < 0.05$. (**F**) Representative photomicrographs of aortic cross sections from wild-type and *Klf15*$^{-/-}$ mice after normal saline or AngII infusion stained with antibody against CD34 (green) to identify adventitial capillaries and DAPI (blue) to identify nuclei. White arrowheads designate adventitial capillaries. Scale bars, 50 μm.

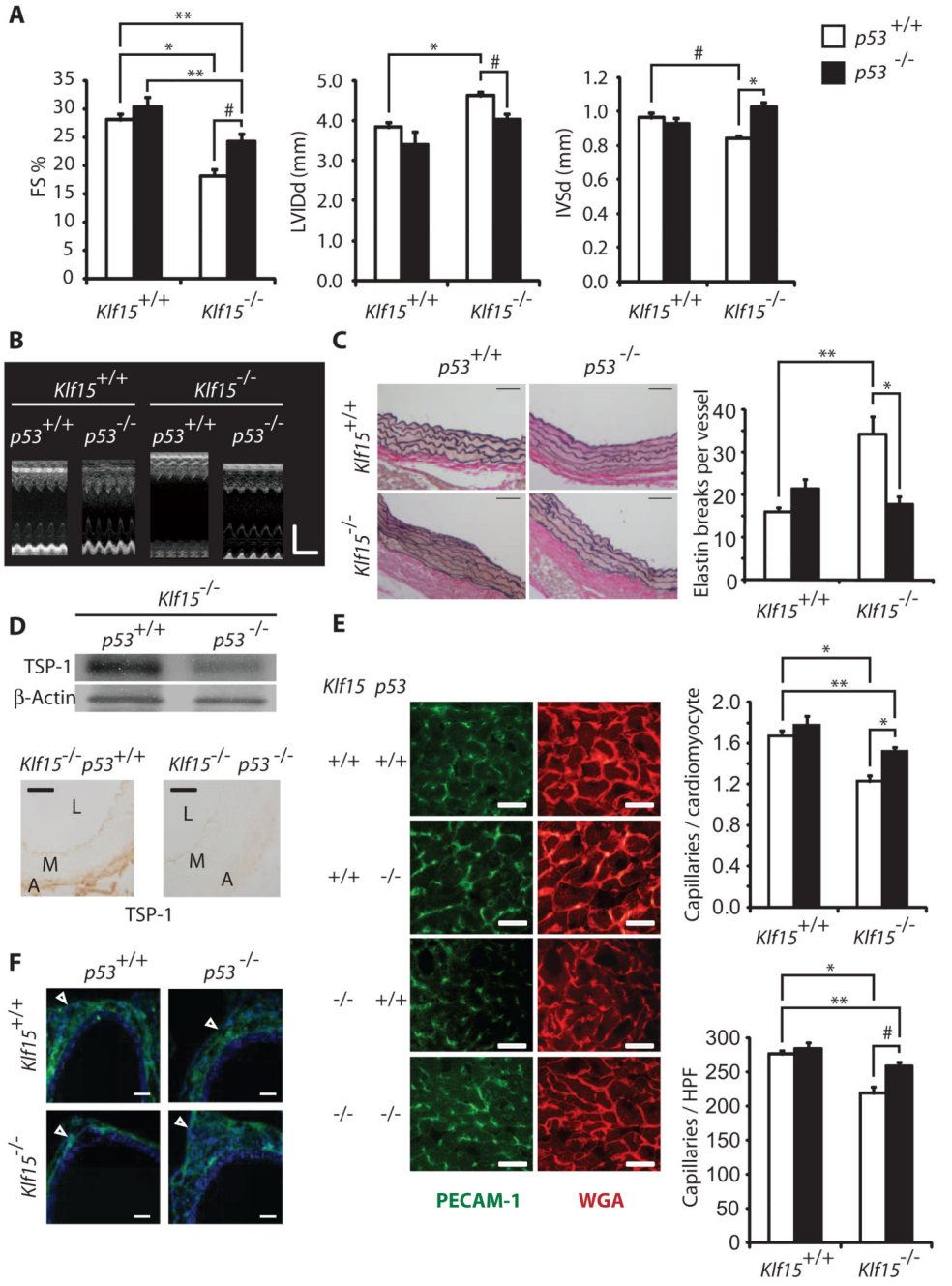

Fig. 4.

Germline deficiency of *p53* rescues heart failure and aortopathy in *Klf15*$^{-/-}$ mice. (**A**) FS, LVIDd, and IVSd of the designated genotypes after AngII infusion (n = 4 to 6 per genotype). *P < 0.001, **P < 0.05, $^{\#}P$ < 0.01. (**B**) Representative M-mode echocardiographic images from the designated genotypes after AngII infusion. Vertical scale bar, 2 mm; horizontal scale bar, 2 ms. (**C**) Representative photomicrographs of elastin-stained aortic cross sections from designated genotypes after AngII infusion (left) with quantification of elastin degradation (right) (n = 4 to 6 per genotype). Scale bars, 50 μm. *P < 0.005, **P < 0.05. (**D**) Western blot of TSP-1 and β-actin from whole-heart lysates (top) and TSP-1 immunostaining of aortic cross sections (bottom) from designated genotypes

after AngII infusion. Scale bars, 50 μm. (**E**) Representative photomicrographs of LV cross sections from designated genotypes after AngII infusion stained with antibody against PECAM-1 (green) to identify intramyocardial vessels and WGA-rhodamine (red) to outline cardiomyocytes. Quantification of capillary density normalized per cardiomyocyte (top) or per 400× HPF (bottom) (n = 4 to 6 per genotype). Scale bars, 50 μm. *$P < 0.001$, **$P < 0.05$, $^{\#}P < 0.003$. (**F**) Representative photomicrographs of aortic cross sections from designated genotypes after AngII infusion immunostained with antibody against CD34 (green) to identify adventitial capillaries and DAPI (blue) to identify nuclei. White arrowheads designate adventitial capillaries. Scale bars, 50 μm.

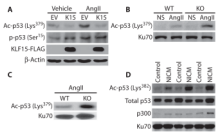

Fig. 5.

KLF15 inhibits p53 acetylation. (**A**) Western blot of acetyl p53 (Ac-p53) (Lys^{379}), phospho-p53 (p-p53) (Ser^{15}), KLF15-FLAG, and β-actin from NRVM infected with control virus (EV) or Ad-KLF15 (K15) and then stimulated with vehicle or AngII. (**B**) Western blot of acetyl p53 (Lys^{379}) and Ku70 (loading) from heart nuclear extracts of wild-type and *Klf15*$^{-/-}$ mice after normal saline or AngII infusion. (**C**) Western blot of acetyl p53 (Lys^{379}) and Ku70 from wild-type and *Klf15*$^{-/-}$ primary aortic smooth muscle nuclear protein after AngII stimulation. (**D**) Western blot of acetyl p53 (Lys^{382}), total p53, p300, and Ku70 from human LV nuclear extracts of control and NICM subjects.

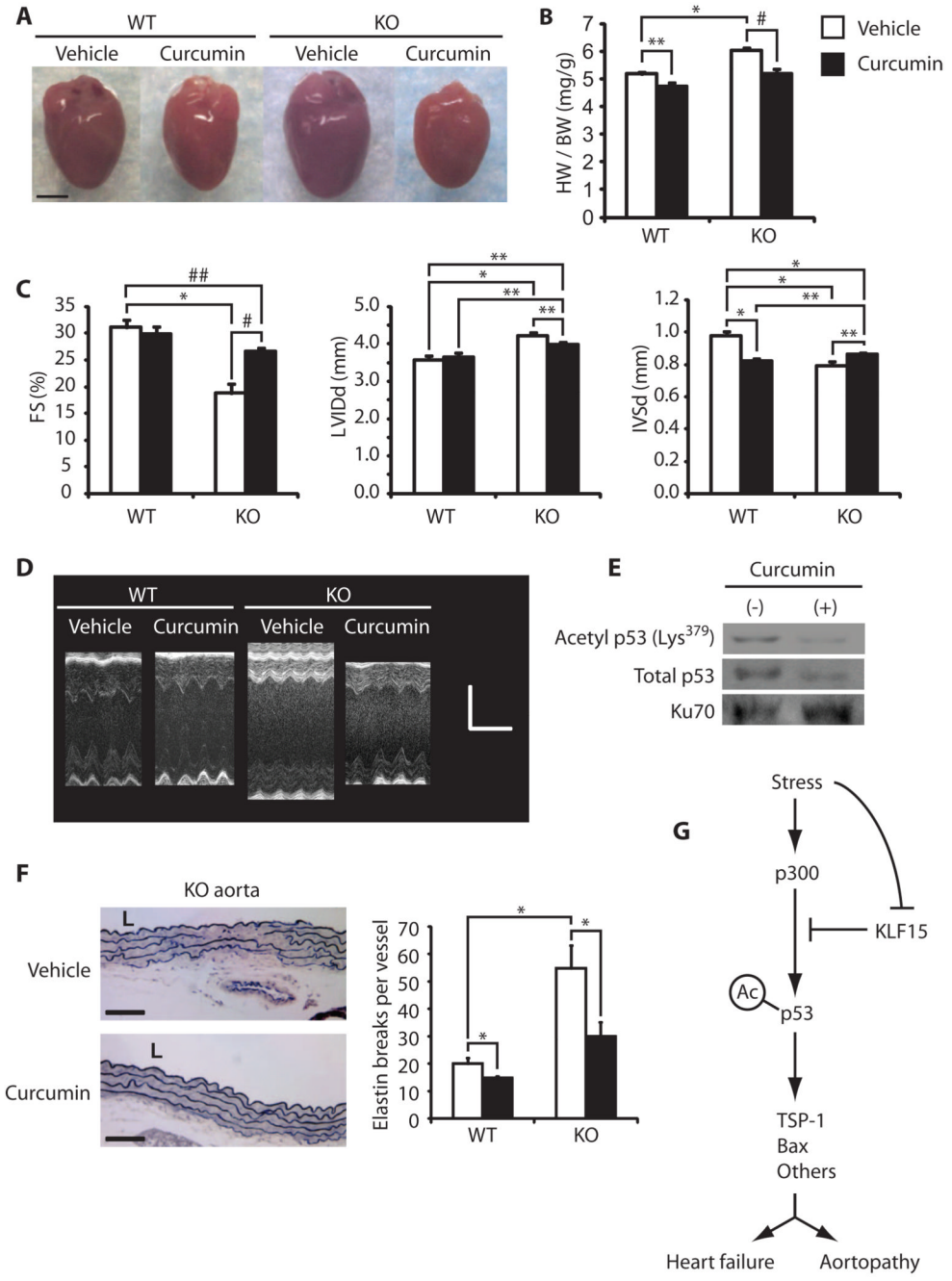

Fig. 6.

Pharmacologic inhibition of p300 rescues heart failure and aortopathy in *Klf15*$^{-/-}$ mice. (**A**) Photographs of freshly excised hearts from curcumin- and vehicle-treated wild-type and *Klf15*$^{-/-}$ mice after AngII infusion. Scale bar, 2.5 mm. (**B**) Heart gravimetry (n = 6 to 8 per group). *P < 0.001, **P < 0.04, $^{\#}P$ < 0.002. HW, heart weight; BW, body weight. (**C**) FS, LVIDd, and IVSd in vehicle- and curcumin-treated wild-type and *Klf15*$^{-/-}$ mice infused with AngII (n = 6 to 8 per group). *P < 0.001, **P < 0.05, $^{\#}P$ < 0.003, $^{\#\#}P$ < 0.02. (**D**) Representative M-mode echocardiographic images from curcumin- and vehicle-treated wild-type and *Klf15*$^{-/-}$ mice after AngII infusion. Vertical scale bar, 2 mm; horizontal scale bar, 2 ms. (**E**) Western blot of acetyl p53 (Lys^{379}), total p53, and Ku70 from heart nuclear

extracts of AngII-infused *Klf15*$^{-/-}$ mice treated with vehicle or curcumin. (**F**) Representative photomicrographs of elastin-stained aortic cross sections from AngII-infused *Klf15*$^{-/-}$ mice treated with vehicle or curcumin (left). Scale bar, 50 μm. (Right) Quantification of elastin degradation (n = 6 to 8 per group). *P < 0.02. (**G**) Schematic of proposed mechanism.